Comparison of Surface Permanent Magnet Coaxial and Cycloidal Radial Flux Magnetic Gears

Matthew C. Gardner
Dept. of Elec. And Comp. Engr.
Texas A&M University
College Station, Texas 77843
gardner1100@tamu.edu

Matthew Johnson
Dept. of Elec. And Comp. Engr.
Texas A&M University
College Station, Texas 77843
mjohnson11@tamu.edu

Hamid A. Toliyat
Dept. of Elec. And Comp. Engr.
Texas A&M University
College Station, Texas 77843
toliyat@tamu.edu

***Abstract*—Magnetic gears transform power between low-torque, high-speed rotation and high-torque, low-speed rotation using magnetic fields instead of interlocking teeth. This paper uses an extensive parametric finite element analysis study to quantitatively compare the optimal performances of two of the most promising magnetic gear topologies, radial flux coaxial magnetic gears and radial flux cycloidal magnetic gears, in terms of volumetric torque density and permanent magnet gravimetric torque density. At low gear ratios, optimal coaxial gears generally achieve higher torque densities than optimal cycloidal gears. However, at medium and high gear ratios, the cycloidal topology can generally outperform the coaxial topology in both of these metrics unless very thick magnets are used. Additionally, the cycloidal magnetic gear can realistically achieve much higher gear ratios than the coaxial magnetic gear, but the optimal gear ratio for a cycloidal design varies with other design parameters, such as outer radius. However, cycloidal designs suffer from significant fabrication challenges because one rotor's axis orbits the axis of the other rotor. Additionally, cycloidal magnetic gear rotors experience strong magnetic forces, which must be supported by the bearings, whereas the net magnetic forces on each rotor in a coaxial magnetic gear can be canceled out using symmetry.**

Keywords—coaxial magnetic gear, cycloidal magnetic gear, finite element analysis, magnet utilization, magnetic force, magnetic gear, permanent magnet, radial flux, torque density, torque ripple

I. Introduction

Like mechanical gears, magnetic gears transform power between low-speed, high-torque rotation and high-speed, low-torque rotation. However, magnetic gears accomplish this power transformation without relying on physical contact between the rotors, using magnetic fields instead of mechanically interlocking teeth. This provides magnetic gears with a plethora of potential advantages over mechanical gears, including improved reliability, reduced maintenance, reduced acoustic noise, and inherent overload protection. Thus, magnetic gears have recently attracted significant interest [1]-[4] and have been proposed for several applications, including wind energy [5], [6], wave energy [7], [8], ship propulsion [9], and traction [10]. The radial flux coaxial magnetic gear, which is illustrated in Fig. 1(a), has received most of the recent attention [1]-[10]. However, the radial flux cycloidal magnetic gear, which is illustrated in Fig. 1(b), has also been the subject of some studies which tout its ability to achieve high torque densities and high gear ratios [11]-[14]. This paper provides a thorough comparison of the two topologies.

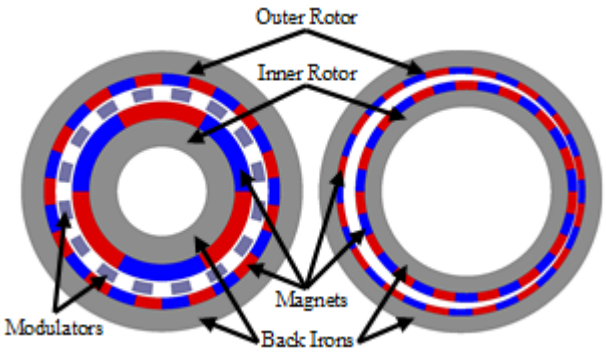

Fig. 1. (a) Coaxial and (b) cycloidal radial flux magnetic gears with surface permanent magnets.

Although the two topologies have significant differences, they rely on similar underlying operating principles: the differing permanent magnet (PM) pole counts on the inner and outer rotors are able to produce the spatial flux harmonics necessary to achieve the gearing behavior due to the spatial harmonics of the air gap permeance function. In coaxial gears, the ferromagnetic modulators placed between the inner and outer rotors create these permeance harmonics, as explained in [1]. For optimal operation, the number of modulators (Q_M) should be equal to the sum of the pole pairs on the inner rotor (P_{In}) and the pole pairs on the outer rotor (P_{Out}), as given by

$$Q_M = P_{In} + P_{Out}. \tag{1}$$

While multiple modes of operation are possible, the highest gear ratio and the highest low speed rotor stall torque are obtained by fixing the outer rotor and allowing the modulator structure and inner rotor to rotate about their common axis. Then, the inner rotor serves as the high speed rotor, and the modulator assembly serves as the low speed rotor, with the gear ratio (G) given by

$$G = \frac{\omega_{In}}{\omega_{Mods}} = \frac{Q_M}{P_{In}}, \tag{2}$$

where ω_{In} and ω_{Mods} are the steady-state speeds of the inner rotor and modulator assembly, respectively.

This work was supported in part by a Texas A&M Energy Institute Fellowship.

In cycloidal gears, the non-uniform, time-varying air gap creates the permeance harmonics, as explained in [11]. Unlike the coaxial gear, the cycloidal gear's rotors are not centered about the same axis. Instead, the inner rotor's axis is parallel to, but offset from the outer rotor's axis, and it moves in an orbital revolution around the outer rotor's stationary central axis. This orbital motion rotates the air gap permeance function, which modulates the spatial flux harmonics to facilitate the gearing behavior. Since the fundamental spatial harmonic of the air gap is unity, the inner and outer rotor pole pairs should be related by

$$P_{Out} = P_{In} + 1 \tag{3}$$

for optimal operation, as indicated in [12]. The orbital revolution is connected to the high speed shaft. The low speed rotation can be provided by either the inner rotor or the outer rotor rotating about its own axis, but it is probably most practical to keep the outer rotor stationary and connect the rotation of the inner rotor about its own axis to the low speed shaft. This yields the gear ratio given by

$$G = \frac{\omega_{Orb}}{\omega_{In}} = -P_{In}, \tag{4}$$

where ω_{Orb} is the speed of the inner rotor's orbital revolution about the outer rotor's axis and ω_{In} is the speed of the inner rotor's rotation about its own axis. The negative sign in (4) indicates that the shafts will rotate in opposite directions. This operation is directly analogous to a mechanical cycloidal drive and is illustrated in Fig. 2, which demonstrates that the inner rotor completes one clockwise orbital revolution about the outer rotor's axis in the same time that the inner rotor rotates one pole pair pitch about its own axis. The gear in Fig. 2 uses 12 inner pole pairs; therefore, for each step in Fig. 2, the inner rotor rotates 3.75° counterclockwise about its own axis, while its own axis orbits 45° clockwise about the outer rotor's axis.

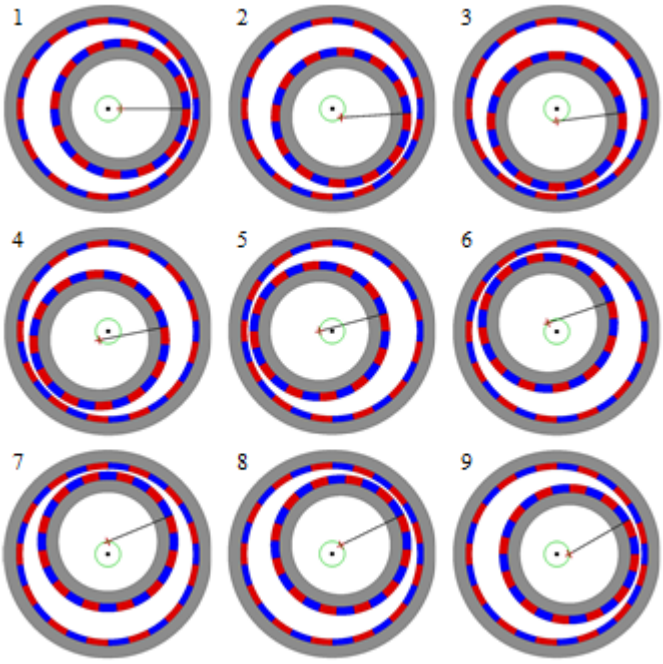

Fig. 2. Example cycloidal magnetic gear operation motion sequence. The inner rotor's axis (red '+') orbits the outer rotor's axis (black dot) along the green path while the inner rotor rotates about its own axis.

A comparison of the gear ratio expressions in (2) and (4) suggests that it is generally more practical to achieve a higher gear ratio with the cycloidal gear than with the coaxial gear because there are practical limitations to the maximum number of modulators or poles that can be used on a rotor. While relatively high gear ratios can be achieved by using coaxial magnetic gears with $P_{In} = 1$, this generally results in relatively high torque ripple [5]. Additionally, a few papers [11]-[13] state that cycloidal magnetic gears can achieve higher torque densities than coaxial magnetic gears. Furthermore, one paper [12] also claims that cycloidal magnetic gears can achieve better magnet utilization than coaxial magnetic gears.

While these foundational cycloidal magnetic gear studies [11]-[14] do an excellent job of introducing the cycloidal magnetic gear topology, explaining its operating principle, demonstrating its potential for high torque densities at high gear ratios, and even describing working prototypes, their comparisons of coaxial and cycloidal magnetic gears' torque density capabilities are based on theoretical observations and anecdotal comparisons of individual designs or extremely limited optimizations, rather than thorough numerical comparisons of the topologies. As an example, [12] describes an un-optimized radial flux cycloidal magnetic gear prototype design constructed using the same number of outer rotor pole pairs and approximately the same air gap radius as the un-optimized coaxial magnetic gear described in [2]. While the cycloidal magnetic gear design in [12] achieves approximately double the torque density of the coaxial gear design in [2], this comparison is of limited value without some measure of the relative optimizations of the two designs, especially since they use the same outer rotor pole pair count, which is unlikely to be equally optimal for both of the different topologies. If one design is very sub-optimal while the other is nearly optimal, this can bias the comparison heavily in favor of the more optimal design. Furthermore, [12] also describes a very limited cycloidal magnetic gear optimization study using an analytical model which achieves a volumetric torque density of 183 kN·m/m^3 and states that this is almost twice the commonly cited typical radial flux coaxial magnetic gear volumetric torque density of 100 kN·m/m^3 provided in [1]. However, this study only considers a single pole pair combination for the cycloidal gear (pole pair counts are an extremely important design parameter as demonstrated in this study), and multiple more recent studies have demonstrated that the radial flux coaxial magnetic can achieve significantly higher torque densities than the 100 kN·m/m^3 figure, depending on the design constraints [3], [7], [15], [16]. This paper builds upon these studies, which clearly demonstrate the radial flux cycloidal magnetic gear's tremendous potential for high torque densities at high gear ratios, by providing the first extensive parametric 2D and 3D finite element analysis (FEA) design study comparing the optimum magnetic performance potentials of the radial flux versions of the two topologies to produce thorough quantitative assessments of their relative capabilities and characterizations of their respective design trends.

II. Design Study Methodology

The two primary metrics considered in this study are volumetric torque density (VTD) and PM gravimetric torque

density (PM GTD). VTD is defined as the low speed rotor stall torque (τ_{LSR}) divided by the active volume, as given by

$$\text{VTD} = \frac{\tau_{LSR}}{\pi \cdot R_{Out}^2 \cdot H}, \quad (5)$$

where R_{Out} is the outer radius of the outer rotor back iron and H is the stack length. Similarly, PM GTD is defined as the low speed rotor stall torque divided by the total mass of the gear PMs, which provides a practical quantitative measure of each design's magnet utilization.

Both topologies were simulated using FEA. For both topologies, the back irons are made from M47 steel, and the PMs are made from NdFeB N42 with a remanence of 1.3 T. The modulators in the coaxial magnetic gear are also made from M47 steel. Table I shows the design parameter values considered for each of the two topologies, excluding the inner pole pair counts, and Tables II and III show the inner pole pair counts evaluated for the two topologies. The inner pole pair counts specified in Tables II and III for the coaxial gear were selected to ensure that that the optimal values for both VTD and PM GTD were always inside the range considered, since the outer radius, air gap size, and gear ratio can significantly affect these values. The same set of inner pole pair counts was always considered for the cycloidal designs, since the inner pole pair count directly determines a cycloidal design's gear ratio according to (4). This range also includes the optimal inner pole pair count with respect to both VTD and PM GTD for all evaluated cycloidal gear designs. A derived parameter, k_{PM}, is used to control the ratio between the PM thicknesses on the two rotors, as given by

$$T_{PM2} = k_{PM} \cdot T_{PM1}, \quad (6)$$

where T_{PM1} and T_{PM2} are the radial thicknesses of the PMs on the inner and outer rotors, respectively. The k_{PM} range given for the coaxial topology in Table I is based on the optimal values indicated by the studies in [15], [16]. For the coaxial gear, G_{Int} is a derived parameter which represents the integer part of the desired gear ratio and is used to maintain an approximately constant target gear ratio while varying the inner rotor pole count, as shown in

$$P_{Out} = \begin{cases} (G_{Int} - 1) \cdot P_{In} + 1 & \text{for } G_{Int} \cdot P_{In} \text{ odd} \\ (G_{Int} - 1) \cdot P_{In} + 2 & \text{for } G_{Int} \cdot P_{In} \text{ even} \end{cases}. \quad (7)$$

Using (7) avoids coaxial designs with integer gear ratios, which are prone to very large torque ripples [5], and coaxial designs with an odd number of modulators, which have unbalanced magnetic forces acting on each rotor. The outer rotor pole pair counts are determined by (7) and (3) for the coaxial and cycloidal topologies, respectively. For each coaxial design, the inner and outer air gap each have the same thickness, T_{AG}. All possible combinations of the parameter values listed in Tables I, II, and III were evaluated using 2D FEA, except for cases which would result in a negative inner radius. Based on the 2D FEA simulation results, the best 906 coaxial designs and 6678 cycloidal designs were evaluated at each of the stack lengths specified in Table I using 3D FEA. The results presented in the next section are based on 3D FEA for designs with stack lengths of 50 mm, except where specified otherwise.

TABLE I. PARAMETER SWEEP VALUES

Parameter	Coaxial	Cycloidal
Integer part of gear ratio (G_{Int})	4, 9, 16	N/A
Outer radius (R_{Out})	50, 75, 100, 150 mm	
Inner back iron thickness (T_{BI1})	5, 10, 20 mm	
Outer back iron thickness (T_{BI2}) For T_{BI1} = 5 mm For T_{BI1} = 10 mm For T_{BI1} = 20 mm	 5 mm 5, 10 mm 5, 10, 20 mm	
Inner PM thickness (T_{PM1})	3, 6, 9, 12, 15 mm	
PM thickness ratio (k_{PM})	0.5, 0.625, 0.75	0.5, 0.625, … 1
Minimum air gap thicknesses (T_{AG})	1 mm, R_{Out}/50	
Axis Offset (T_{Off})	N/A	1,2,3,4,5,7,10 mm
Modulator thickness (T_{Mods})	10 mm	N/A
Stack Length (L_{Stack})	5, 10, 20, 30, 50 mm	

TABLE II. INNER POLE PAIR COUNT (P_{In}) VALUES WITH T_{AG} = 1 mm

R_{Out} (mm)	Coaxial (G_{Int} = 4)	Coaxial (G_{Int} = 9)	Coaxial (G_{Int} = 16)	Cycloidal
50	3, 5, 7	3, 5, 7	3, 5	5, 9, … 89
75	3, 5, 7, 9	3, 5, 7	3, 5	5, 9, … 89
100	3, 5, 7, … 17	3, 5, 7, 9, 11	3, 5, 7	5, 9, … 89
150	3, 5, 7, … 21	3, 5, 7, … 13	3, 5, 7, 9	5, 9, … 89

TABLE III. INNER POLE PAIR COUNT (P_{In}) VALUES WITH $T_{AG} = R_{Out}/50$

R_{Out} (mm)	Coaxial (G_{Int} = 4)	Coaxial (G_{Int} = 9)	Coaxial (G_{Int} = 16)	Cycloidal
50	3, 5, 7	3, 5, 7	3, 5	5, 9, … 89
75	3, 5, 7, 9	3, 5, 7	3, 5	5, 9, … 89
100	3, 5, 7, 9	3, 5, 7	3, 5	5, 9, … 89
150	3, 5, 7, 9, 11	3, 5, 7	3, 5	5, 9, … 89

III. DESIGN STUDY RESULTS

Figs. 3 – 5 illustrate several design trends for the coaxial and cycloidal magnetic gears. Fig. 4 compares the maximum VTDs and PM GTDs that both topologies achieve at different outer radii. With a fixed air gap, the VTD and PM GTD both increase with the outer radius for both topologies (assuming that the cycloidal gear ratio is allowed to vary, as in the black curves in Figs. 3-5). However, when the air gap increases proportionally with the outer radius, both VTD and PM GTD vary much less with the outer radius for both topologies, but there is more variation for the cycloidal topology than for the coaxial topology, due in part to the fact that cycloidal gears only have a single air gap. Fig. 4 also illustrates that at lower gear ratios, optimal coaxial gears tend to achieve higher VTDs and PM GTDs than optimal cycloidal gears, and this advantage increases as the permissible outer radius increases. This is because a range of inner rotor pole pair counts can be used to achieve similar gear ratios for the coaxial gear (thus providing the freedom to optimize this important design parameter), but a given inner rotor pole pair value directly determines a cycloidal design's gear ratio. However, the coaxial topology's achievable VTD and PM GTD tend to decrease significantly as the gear ratio is increased (due to the increased discrepancy between the inner and outer rotor magnet pole counts and pole arcs). Accordingly,

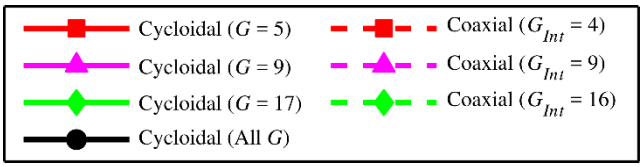

Fig. 3. Legend for Figs. 4 and 5. (Each curve is based on 3D FEA for designs with 50 mm stack lengths.)

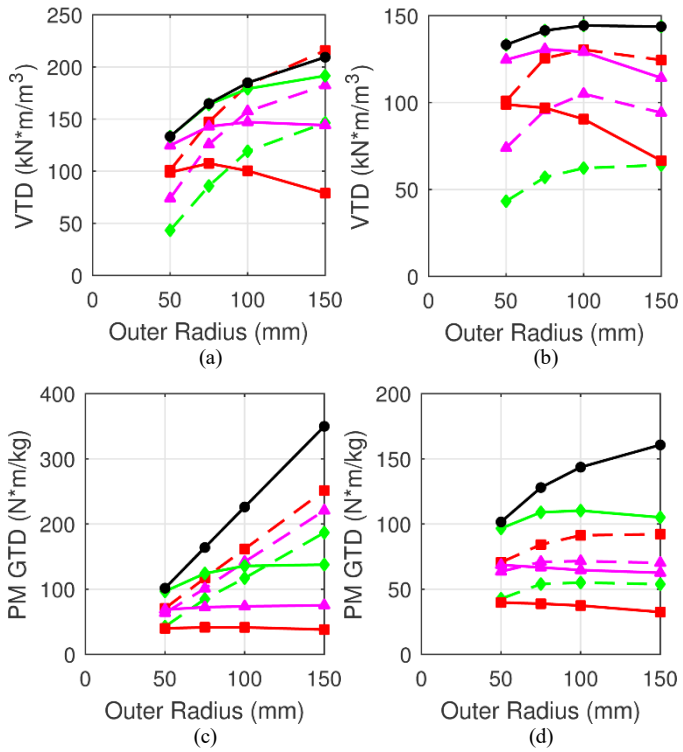

Fig. 4. Variation of the maximum VTD with outer radius for designs with (a) T_{AG} = 1 mm and (b) T_{AG} = R_{Out}/50 and variation of the maximum PM GTD with outer radius for designs with (c) T_{AG} = 1 mm and (d) T_{AG} = R_{Out}/50.

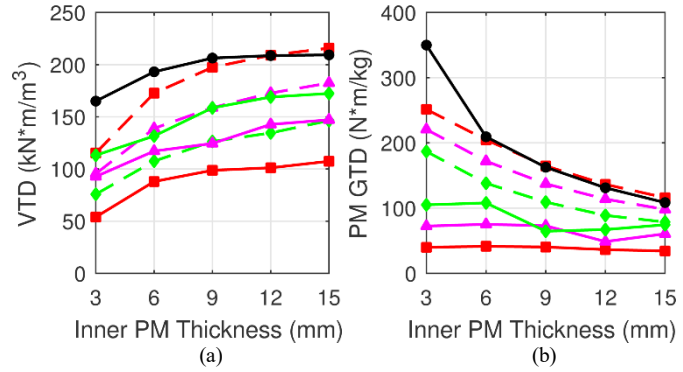

Fig. 5. Variation of the maximum (a) VTD and (b) PM GTD with the inner rotor PM thickness for designs with R_{Out} = 150 mm and T_{AG} = 1 mm.

at medium to high gear ratios, unless the magnets are very thick and the air gaps relatively small, optimal coaxial designs tend to achieve lower VTDs and PM GTDs than optimal cycloidal designs. Furthermore, if any cycloidal gear ratio is permissible (corresponding to the black curves in Figs. 3-5), then the cycloidal topology can generally achieve higher torque densities than the coaxial topology at most design points in this study.

Fig. 5 illustrates the impact of the inner rotor magnet thickness on VTD and PM GTD. For both topologies, within the evaluated range of thicknesses, VTD increases as the inner PM thickness is increased, whereas PM GTD decreases as the inner PM thickness is increased. However, as the PM thickness increases, the coaxial topology tends to benefit more in terms of VTD and suffer less in terms of PM GTD than the cycloidal topology.

For the coaxial topology, the optimal gear performance is generally achieved with a relatively low gear ratio [7]. However, for the cycloidal topology, the optimal gear ratio varies significantly based on the other design criterion. Fig. 6 illustrates how the optimal gear ratio changes with outer radius. The gear ratio for maximizing PM GTD is generally higher than the gear ratio for maximizing VTD. This is because maximum PM GTD designs favor thinner magnets (and thus smaller effective air gaps), which can tolerate higher pole counts and shorter pole arcs without suffering from reduced torque densities due to increased tangential leakage flux [7], [15], [16]. Additionally, the optimal gear ratio tends to increase with the outer radius but decrease as the air gap increases. This is because the increased air gap leads to increased leakage flux per pole, which can be counteracted by lower pole counts and longer pole arcs. Another important parameter that affects both the achievable performance and the optimal gear ratio of the cycloidal magnetic gear is the offset between the axes of the inner and outer rotors. As shown in Fig. 7, the optimal gear ratio tends to decrease significantly as the axis offset increases. Again, this is partially because a larger axis offset leads to a

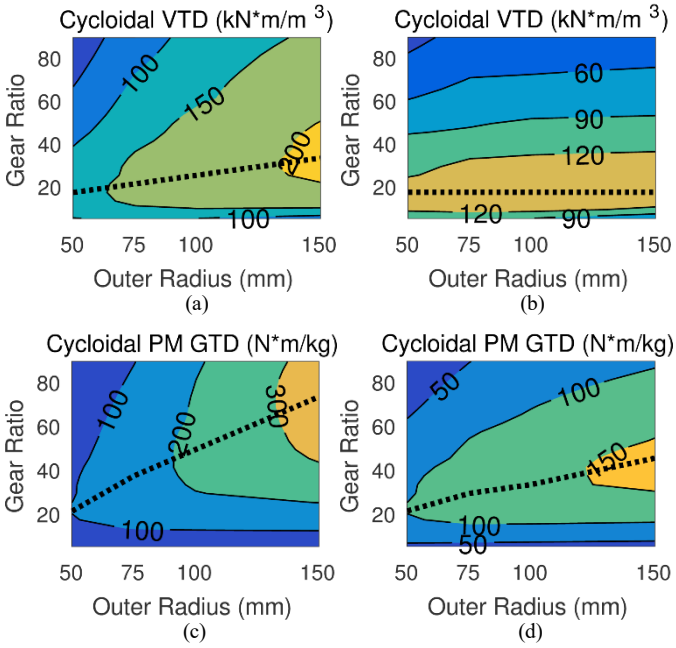

Fig. 6. Variation of the maximum VTD with outer radius and gear ratio for cycloidal designs with (a) T_{AG} = 1 mm and (b) T_{AG} = R_{Out}/50 and variation of the maximum PM GTD with outer radius and gear ratio for cycloidal designs with (c) T_{AG} = 1 mm and (d) T_{AG} = R_{Out}/50. The dotted line indicates the gear ratio that maximizes VTD or PM GTD for each outer radius.

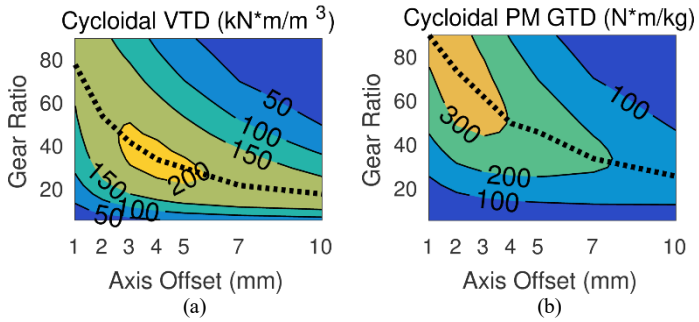

Fig. 7. Variation of the maximum (a) VTD and (b) PM GTD with the axis offset and gear ratio for cycloidal designs with R_{Out} = 150 mm and T_{AG} = 1 mm. The dotted line indicates the gear ratio that maximizes VTD or PM GTD for each axis offset.

larger average effective air gap, which leads to more leakage flux per pole if the pole arc lengths are not increased.

Another important factor that impacts magnetic gear performance is end-effects. Fig. 8 compares the maximum achievable VTDs for designs with different stack lengths based on both 2D and 3D FEA. Fig. 8 shows a greater discrepancy between 2D and 3D FEA for the coaxial designs than for the cycloidal designs, which means that the coaxial designs suffer

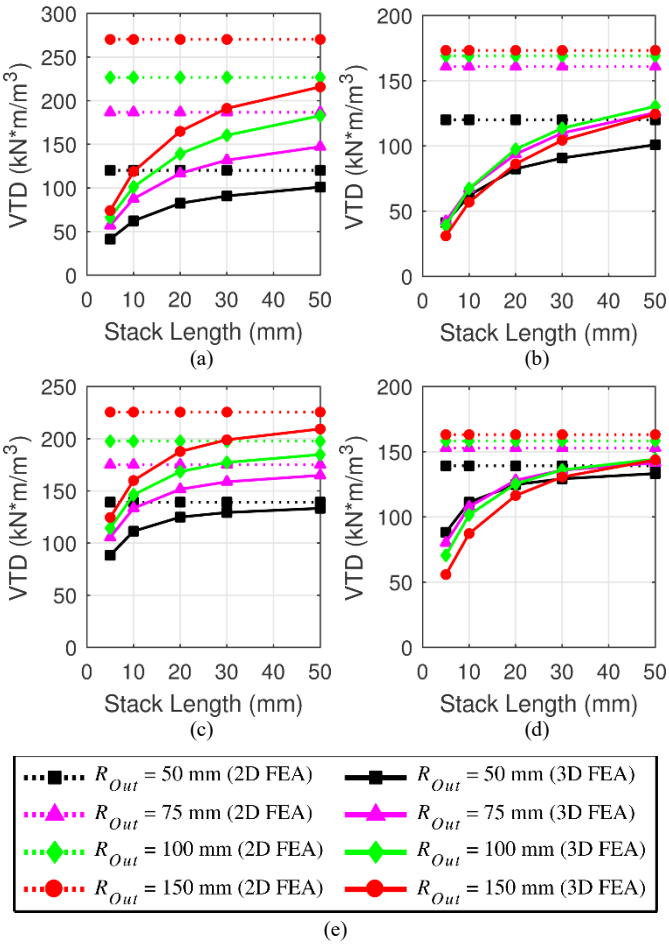

Fig. 8. Variation of the maximum VTD with the stack length for (a) coaxial designs with T_{AG} = 1 mm, (b) coaxial designs with $T_{AG} = R_{Out}/50$, (c) cycloidal designs with T_{AG} = 1 mm, and (d) cycloidal designs with $T_{AG} = R_{Out}/50$ for (e) different outer radii based on both 2D and 3D FEA.

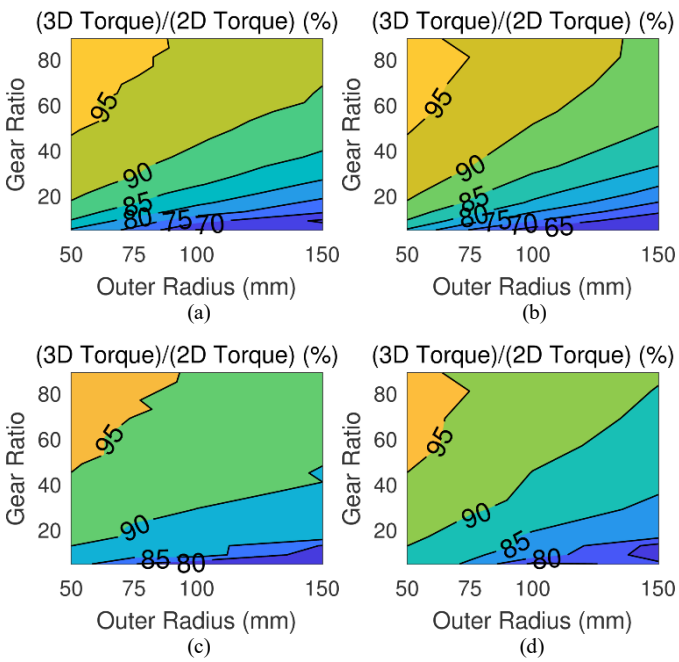

Fig. 9. Variation of 3D end-effects on the maximum VTD designs of Fig. 6, but at a stack length of 20 mm, with outer radius and gear ratio for cycloidal designs with (a) T_{AG} = 1 mm and (b) $T_{AG} = R_{Out}/50$, and variation of the 3D end-effects of the maximum PM GTD designs from Fig. 6, but at a stack length of 20 mm, with outer radius and gear ratio for cycloidal designs with (c) T_{AG} = 1 mm and (d) $T_{AG} = R_{Out}/50$.

more from end-effects, likely due to the phenomenon of escaping flux in coaxial magnetic gears [16], [17]. Additionally, the higher pole counts favored by cycloidal designs inherently lead to shorter flux paths and reduced end-effects, as demonstrated by the graphs in Fig. 9 which indicate that cycloidal designs suffer smaller torque reductions due to end-effects at higher gear ratios (and, thus, higher pole counts). This difference in end-effects also means that the VTD and PM GTD advantages of the cycloidal topology over the coaxial topology will become more significant in applications requiring a smaller stack length, but these advantages will be reduced for applications requiring a larger stack length.

IV. The Spatial Distribution of Torque Production

The previous section numerically illustrates differences in design trends between the two topologies. Some of these differences can be explained by considering an approximate analysis of the spatial distribution of torque production in the cycloidal topology. This analysis is based on a couple of simplifying assumptions, which make its implications more intuitive but prevent it from being used for exact analysis. First, only the fundamental harmonics from the PMs on the inner and outer rotors are considered, and other spatial magnetomotive force (mmf) harmonics are neglected. Second, the torque distribution at any angle, θ, from the axis of the outer rotor is proportional to the sine of the difference between the electromagnetic angles of the two rotors, k_τ, as given by

$$k_\tau = \sin(P_{In} \cdot \theta' - P_{Out} \cdot \theta + \theta_{EM1} - \theta_{EM2}), \quad (8)$$

where θ_{EM1} and θ_{EM2} are the electromagnetic angles of the inner and outer rotors at θ = 0. Note that θ' represents the angle from

the axis of the inner rotor, which will be slightly different than θ due to the cycloidal gear's axis offset. Fig. 10(a) plots both k_τ and the inverse effective air gap function, g^{-1}, as functions of θ for an example cycloidal magnetic gear, and Fig. 10(b) illustrates k_τ as the color in the air gap of the example cycloidal magnetic gear. (Note that the thicknesses of the PMs on the two rotors are included in the effective air gap.)

When a cycloidal magnetic gear is at its maximum torque orientation, as shown in Fig. 10, positive torque is being produced in the area with the smallest air gap, and negative torque is being produced in the area with the largest air gap. However, as the PM thicknesses increase, the effective air gap increases. To maintain the same ratio between the maximum and minimum values of the effective air gap, the axis offset must increase, as demonstrated in Fig. 11. While increasing the axis offset reduces the negative torque produced in the region where k_τ is negative, it also increases the air gap in much of the region where k_τ is positive, which reduces the positive torque produced. On the other hand, in the coaxial magnetic gear, the modulators allow discrete steps in the effective air gap function. This contrast explains why increasing the PM thickness is more beneficial to the coaxial topology in terms of VTD and less detrimental to the coaxial topology in terms of PM GTD.

This analysis also provides a partial explanation for why higher pole counts favor smaller axis offsets for the cycloidal gear. As the pole count increases, the flux paths become shorter. Thus, the axis offset must be reduced to maintain the same torque production in the regions where k_τ is positive; furthermore, because of these shorter flux paths, this reduction of the axis offset will not result in a large increase in the negative

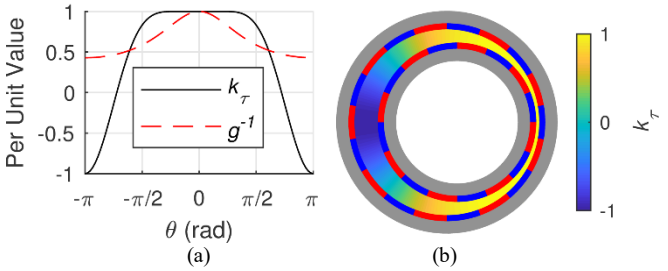

Fig. 10. (a) Variation of k_τ and the inverse effective air gap function (both in per unit values) with spatial position in an example cycloidal magnetic gear and (b) k_τ plotted as the color in the air gap of the same cycloidal magnetic gear.

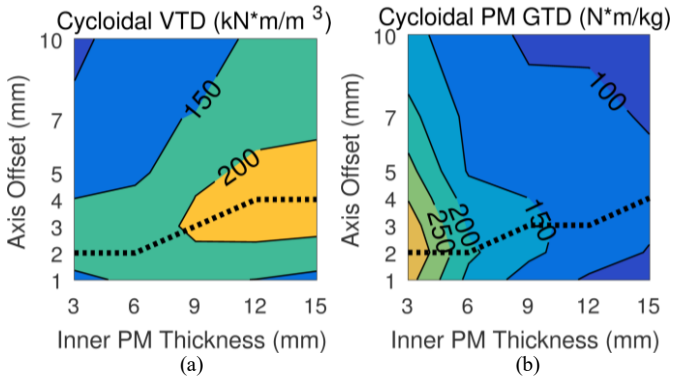

Fig. 11. Variation of the maximum (a) VTD and (b) PM GTD with the inner PM thickness and axis offset for cycloidal designs with R_{Out} = 150 mm and T_{AG} = 1 mm. The dotted line indicates the axis offset that maximizes VTD or PM GTD for each inner PM thickness.

torque produced in regions where k_τ is negative. Another factor driving the optimal axis offset is that the axis offset affects the geometric transformation between θ and θ', which determines how much of the gear is producing positive torque.

V. Rotor Forces and Torque Ripples

Another significant difference between the two topologies is the presence of net magnetic forces on the rotors of the cycloidal topology. Fig. 12 shows the net magnetic forces on the inner rotors of the designs with the highest VTDs and PM GTDs for each outer radius, which correspond to the points in Figs. 4(a) and 4(c). While the cycloidal magnetic gear designs experience significant net magnetic forces, the coaxial designs experience negligible (zero if there are no manufacturing tolerances) net magnetic forces on the rotors due to the symmetry imposed by (7). Fig. 12 also illustrates that the net magnetic forces tend to increase as the outer radius increases, which is largely due to the increase in air gap area. Furthermore, Fig. 12 indicates that the maximum VTD designs have larger net magnetic forces than the maximum PM GTD designs, which is largely due to the thicker PMs of the maximum VTD designs.

Fig. 12 illustrates the net magnetic forces at the maximum torque points for the designs, but the magnetic forces do vary significantly with the operating point. Figs. 13 and 14 illustrate the variation of torques and forces based on 2D FEA as the torque angle changes for the cycloidal designs with the absolute maximum VTD and PM GTD. The torque angle is defined as the difference between the electromagnetic angles of the two rotors at the point where the air gap is minimal. Figs. 13(a) and 13(b) show that the maximum force occurs at the operating point where the torque angle is 0 and there is no torque. Fig. 14 illustrates that the angle of the net magnetic force varies with the torque angle. If too much torque was applied to either shaft and the gear began to slip, the forces on the inner rotor would trace the paths shown in Fig. 14. The bearings on the inner rotor must be able to withstand these magnetic forces, which are significantly larger than the active weight of the inner rotor. For reference, the total combined masses of the back irons and PMs on the inner rotor are about 7.1 kg and 4.2 kg for the maximum VTD and maximum PM GTD designs, respectively.

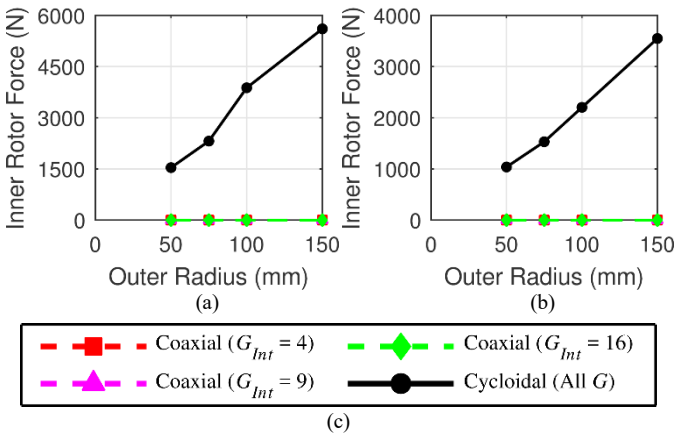

Fig. 12. The net forces on the inner rotor at the maximum torque points of (a) the maximum VTD designs corresponding to the points in Fig. 4(a) and of (b) the maximum PM GTD designs corresponding to the points in Fig. 4(c) for (c) both topologies based on 3D FEA for designs with 50 mm stack lengths.

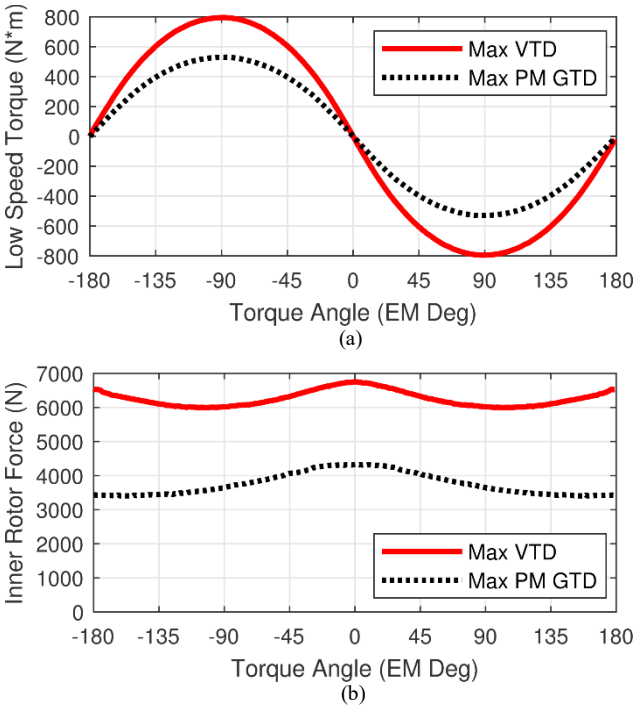

Fig. 13. The 2D FEA variation of (a) low speed shaft torque and (b) net magnetic forces on the inner rotor as the torque angle is varied for the maximum VTD and PM GTD cycloidal designs from the entire simulation study.

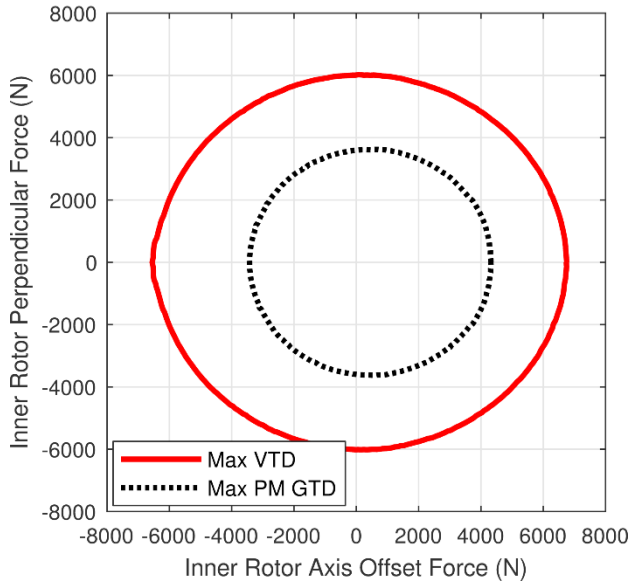

Fig. 14. The variation of the forces in the direction of the axis offset and in the direction perpendicular to the axis offset based on 2D FEA as the torque angle is varied for the maximum VTD and PM GTD cycloidal designs from the entire simulation study.

Fig. 15 illustrates the torque and force ripple characteristics for the same optimal designs used in Figs. 13 and 14 during steady-state operation at the maximum torque angle based on 2D FEA. The rotation angle is defined as the electromagnetic angle which the inner rotor has both simultaneously rotated and orbited in opposite directions. Fig. 15 shows that both designs exhibited negligible torque and force ripples. Additionally, when either gear is operating in steady-state at a constant torque,

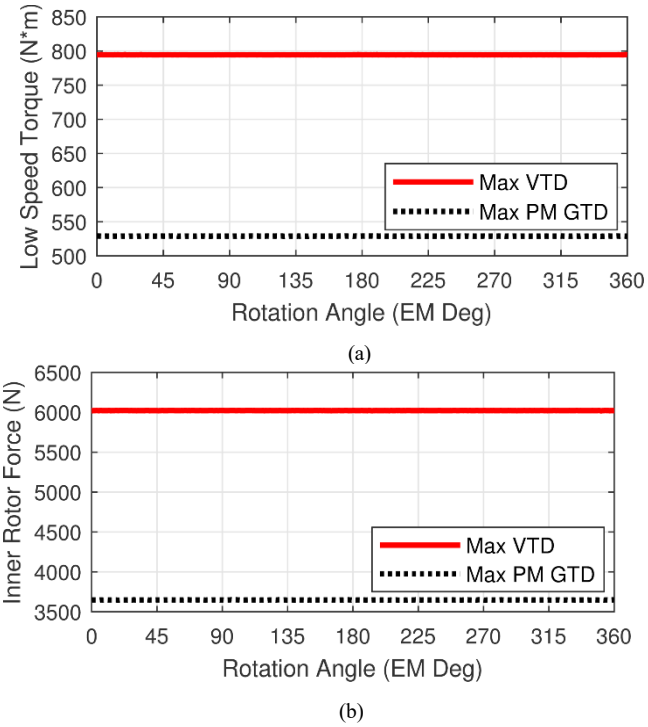

Fig. 15. The variation of the (a) low speed shaft torque and (b) net magnetic forces on the inner rotor based on 2D FEA during steady-state operation at the maximum torque angle for the maximum VTD and PM GTD cycloidal designs from the entire simulation study.

the angle of net magnetic force is fixed with respect to the axis offset. Alternatively, for a coaxial magnetic gear, the net magnetic forces on the rotors and the rotor torque ripples are heavily dependent on the pole pair count selections. Coaxial gears designed with proper symmetry ideally experience zero net magnetic forces on their rotors. Furthermore, coaxial gear designs with relatively high lowest common multiples between P_{In}, P_{Out}, and Q_M and non-integer gear ratios can also achieve very low torque ripples. Both of these conditions can generally be simultaneously achieved by using (7). For example, the coaxial magnetic gear in [7] uses a $P_{In} = 6$, $P_{Out} = 68$ and $Q_M = 74$ design, resulting in simulated peak-to-peak high speed rotor and low speed rotor torque ripples of 2.2% and 0.02%, respectively. However, a nearly identical variation of the design which only changes the pole pair count combinations to $P_{In} = 6$, $P_{Out} = 66$ and $Q_M = 72$, resulting in an integer gear ratio, exhibits significantly larger high speed rotor and low speed rotor torque ripples of 134.5% and 1.88%, respectively.

VI. Conclusion

This study employs an extensive parametric evaluation to quantitatively compare the optimal achievable performances of coaxial magnetic gears and cycloidal magnetic gears in terms of volumetric torque density (VTD) and magnet utilization (PM GTD). Each topology has its own benefits and drawbacks with respect to gear ratio, torque, and mechanical design.

Regarding gear ratio, the cycloidal magnetic gear can realistically achieve significantly higher gear ratios than the coaxial magnetic gear. The coaxial gear generally favors relatively low gear ratios with the performance (torque density)

getting significantly worse as the gear ratio increases. However, the optimal gear ratio for a cycloidal magnetic gear varies significantly with other design parameters, especially the outer radius, because the magnitude of the gear ratio is equivalent to the pole pair count on the inner rotor. Additionally, the cycloidal gear actually performs relatively poorly at low gear ratios, especially at larger outer radii. On the other hand, the coaxial gear consistently performs best at low gear ratios, regardless of outer radius, because both sets of pole counts can be varied with the outer radius without significantly changing the gear ratio.

Regarding torque, the cycloidal magnetic gear can generally outperform the coaxial magnetic gear in terms of both VTD and PM GTD, assuming that the optimal gear ratio is used for the cycloidal magnetic gear. However, if the gear ratio is restricted to a relatively low value, the coaxial topology can generally achieve higher VTD and PM GTD values. Furthermore, the coaxial magnetic gear benefits more in terms of VTD and suffers less in terms of PM GTD when the magnet thicknesses are increased. Thus, a coaxial magnetic gear may be more compact if relatively thick PMs can be used, which may be advantageous when size and mass are more important than material cost, but, when the PM thickness is constrained to limit the material cost, the cycloidal magnetic gear will generally be able to achieve higher VTDs and PM GTDs than the coaxial magnetic gear. For the coaxial magnetic gear, torque ripple can be kept small simply by choosing pole count combinations with a large lowest common multiple. The cycloidal topology itself ensures that the torque ripple in a cycloidal magnetic gear will be minimal, regardless of the pole counts.

Finally, there are significant differences regarding construction. The modulators present a challenge to the fabrication of coaxial magnetic gears because they must be held between the two sets of PMs and withstand strong magnetic forces, which can make it mechanically challenging to maintain small air gaps. The cycloidal magnetic gear also presents a couple of fabrication challenges. First, the axis of the inner rotor revolves around the axis of the outer rotor. This requires that the movement of the inner rotor be separated into two components, its orbital revolution about the axis of the outer rotor and its rotation about its own axis. (The dual-stage solution proposed in [11] does simplify this challenge at the expense of reduced VTD and PM GTD.) Additionally, the revolution of the inner rotor moves the gear's center of mass, which must be counterbalanced to avoid creating vibrations. Second, the rotors in a cycloidal magnetic gear experience strong magnetic forces, which must be supported by the bearings, whereas the net magnetic forces on the rotors of a coaxial magnetic gear can be canceled out using symmetry. The additional stress placed on the bearings of a cycloidal magnetic gear by these magnetic forces and the challenges of the inner rotor's revolution may reduce the reliability, maintenance, and acoustic noise benefits inherent in the noncontact power transmission of magnetic gears and mitigate some of the topology's advantages relative to coaxial gears with respect to achieving high torque densities at high gear ratios.

ACKNOWLEDGMENT

The authors would like to thank ANSYS for their support of the EMPE lab through the provision of FEA software.

REFERENCES

[1] K. Atallah and D. Howe, "A novel high-performance magnetic gear," *IEEE Trans. Magn.*, vol. 37, no. 4, pp. 2844–2846, Jul. 2001.

[2] P. O. Rasmussen, T. O. Anderson, F. T. Jorgensen, and O. Nielsen, "Development of a High Performance Magnetic Gear," *IEEE Trans. Ind. Appl.*, vol. 41, no. 3, pp. 764-770, May/June 2005.

[3] K. K. Uppalapati, J. Z. Bird, J. Wright, J. Pitchard, M. Calvin, and W. Williams, "A magnetic gearbox with an active region torque density of 239Nm/L," *IEEE Trans. Ind. Appl.*, vol. 54, no. 2, pp. 1331-1338, Mar./Apr. 2018

[4] P. M. Tlali, R.-J. Wang, and S. Gerber, "Magnetic gear technologies: A review," in *Proc. Int. Conf. Elect. Mach.*, 2014, pp. 544–550.

[5] N. W. Frank and H. A. Toliyat, "Gearing ratios of a magnetic gear for wind turbines," in *Proc. IEEE Int. Elect. Mach. and Drives Conf.*, 2009, pp. 1224–1230.

[6] L. N. Jian, K. T. Chau, D. Zhang, J. Z. Jiang and Z. Wang, "A Magnetic-Geared Outer-Rotor Permanent-Magnet Brushless Machine for Wind Power Generation," in *Proc. IEEE Ind. Appl. Annual. Meeting*, 2007, pp. 573-580.

[7] M. Johnson, M. C. Gardner, H. A. Toliyat, S. Englebretson, W. Ouyang, and C. Tschida, "Design, Construction, and Analysis of a Large Scale Inner Stator Radial Flux Magnetically Geared Generator for Wave Energy Conversion," *IEEE Trans. Ind. Appl.*, pp. 1-1, 2018.

[8] K. K. Uppalapati, J. Z. Bird, D. Jia, J. Garner, and A. Zhou, "Performance of a magnetic gear using ferrite magnets for low speed ocean power generation," in *Proc. IEEE Energy Convers. Congr. and Expo.*, 2012, pp. 3348–3355.

[9] L. MacNeil, B. Claus, and R. Bachmayer, "Design and evaluation of a magnetically-geared underwater propulsion system for autonomous underwater and surface craft," in *Proc. Int. Conf. IEEE Oceans*, 2014, pp. 1-8.

[10] T. V. Frandsen, L. Mathe, N. I. Berg, R. K. Holm, T. N. Matzen, P. O. Rasmussen, and K. K. Jensen, "Motor integrated permanent magnet gear in a battery electrical vehicle," *IEEE Trans. Ind. Appl.*, vol. 51, no. 2, pp. 1516–1525, Mar./Apr. 2015.

[11] J. Rens, K. Atallah, S. D. Calverley and D. Howe, "A Novel Magnetic Harmonic Gear," *IEEE Trans. Ind. Appl.*, vol. 46, no. 1, pp. 206-212, Jan./Feb. 2010.

[12] F. T. Jorgensen, T. O. Andersen and P. O. Rasmussen, "The Cycloid Permanent Magnetic Gear," *IEEE Trans. Ind. Appl.*, vol. 44, no. 6, pp. 1659-1665, Nov./Dec. 2008.

[13] K. Davey, T. Hutson, L. McDonald and G. Hutson, "The design and construction of cycloidal magnetic gears," in *Proc. IEEE Int. Elect. Mach. And Drives Conf.*, 2017, pp. 1-6.

[14] K. Li, J. Bird, J. Kadel and W. Williams, "A Flux-Focusing Cycloidal Magnetic Gearbox," *IEEE Trans. Magn.*, vol. 51, no. 11, pp. 1-4, Nov. 2015.

[15] M. Johnson, M. C. Gardner, and H. A. Toliyat, "Design Comparison of NdFeB and Ferrite Radial Flux Surface Permanent Magnet Coaxial Magnetic Gears," *IEEE Trans. Ind. Appl.*, vol. 54, no. 2, pp. 1254-1263, Mar./Apr. 2018.

[16] M. C. Gardner, B. E. Jack, M. Johnson, and H. A. Toliyat, "Comparison of Surface Mounted Permanent Magnet Coaxial Radial Flux Magnetic Gears Independently Optimized for Volume, Cost, and Mass," *IEEE Trans. Ind. Appl.*, vol. 54, no. 3, pp. 2237-2245, May/June 2018.

[17] S. Gerber and R-J. Wang, "Analysis of the end-effects in magnetic gears and magnetically geared machines," in *Proc. IEEE Int. Conf. Elect. Mach.*, 2014, pp. 396-402.